Free Radical Biology and Medicine 85 (2015) 228–236

Contents lists available at ScienceDirect

Free Radical Biology and Medicine

journal homepage: www.elsevier.com/locate/freeradbiomed

Original Contribution

Plasmodium falciparum antioxidant protein reveals a novel mechanism for balancing turnover and inactivation of peroxiredoxins

Verena Staudacher [a,1], Carine F. Djuika [a,1], Joshua Koduka [a,1], Sarah Schlossarek [a,1], Jürgen Kopp [b,c], Marleen Büchler [a], Michael Lanzer [a], Marcel Deponte [a,*]

[a] Department of Parasitology, Ruprecht–Karls University, D-69120 Heidelberg, Germany
[b] Biochemistry Center (BZH), Ruprecht–Karls University, D-69120 Heidelberg, Germany
[c] Cellnetworks Excellence Cluster, Ruprecht–Karls University, D-69120 Heidelberg, Germany

ARTICLE INFO

Article history:
Received 11 March 2015
Received in revised form
20 April 2015
Accepted 24 April 2015
Available online 5 May 2015

Keywords:
Peroxiredoxin
Catalytic mechanism
Inactivation
Redox regulation
Molecular evolution

ABSTRACT

Life under aerobic conditions has shaped peroxiredoxins (Prx) as ubiquitous thiol-dependent hydroperoxidases and redox sensors. Structural features that balance the catalytically active or inactive redox states of Prx, and, therefore, their hydroperoxidase or sensor function, have so far been analyzed predominantly for Prx1-type enzymes. Here we identify and characterize two modulatory residues of the Prx5-type model enzyme *Pf*AOP from the malaria parasite *Plasmodium falciparum*. Gain- and loss-of-function mutants reveal a correlation between the enzyme parameters and the inactivation susceptibility of *Pf*AOP with the size of residue 109 and the presence or absence of a catalytically relevant but nonessential cysteine residue. Based on our kinetic data and the crystal structure of *Pf*AOP^{L109M}, we suggest a novel mechanism for balancing the hydroperoxidase activity and inactivation susceptibility of Prx5-type enzymes. Our study provides unexpected insights into Prx structure–function relationships and contributes to our understanding of what makes Prx good enzymes or redox sensors.

Introduction

Peroxiredoxins (Prx) are among the most abundant proteins in a cell and play central roles not only as detoxifying hydroperoxidases but also as redox-regulated chaperones and redox sensors [1–6]. How are these alternative functions balanced? Furthermore, which protein properties determine whether a Prx maintains its enzymatic activity or becomes inactivated? These questions have been adequately addressed for the so-called Prx1-type enzymes with or without an YF motif close to the C-terminus [1,7–15] but remain mostly unanswered for the other five Prx subfamilies.

The human malaria parasite *Plasmodium falciparum* has five different parasite-encoded Prx [16–19] and imports a high-abundant erythrocytic Prx that contributes to hydroperoxide removal [20]. One of the parasite-encoded Prx, the so-called antioxidant protein *Pf*AOP, is a model enzyme for a special subclass of Prx with a high enzymatic activity using glutaredoxin (Grx) and reduced glutathione (GSH) as electron donors [21]. *Pf*AOP has a prokaryotic ancestry and is dual localized to the parasite cytosol and plastid most likely because of a gene fusion event following a horizontal gene transfer [22]. Based on its dimerization site and other structural features, *Pf*AOP belongs to the Prx5-type subfamily of Prx [23–25]. Rather little is known about the physiological relevance and functions of this subfamily. Variants of mammalian Prx5 are found in a number of tissues in mitochondria, peroxisomes, the cytosol, and the nucleus and were reported to prevent mitochondrial DNA damage and to modulate cell death [25–29]. A *prx5–grx* hybrid gene from *Haemophilus influenzae* was shown to be essential for stationary cultures under aerobic but not anaerobic growth conditions [30]. Furthermore, the mechanistically unusual Prx5-type enzyme Ahp1 from yeast was shown to form an intermolecular disulfide bond with the transcription factor Cad1 and to redox-regulate Cad1 in a hydroperoxide-dependent manner [31]. Structural features that balance the redox states and therefore the hydroperoxidase and regulatory functions of Prx5-type enzymes are so far unknown.

The active site of *Pf*AOP contains the essential peroxidatic cysteine residue Cys117, which reacts with the hydroperoxide substrate to a sulfenic acid [21,23]. This rapid oxidative half-reaction has been thoroughly analyzed for human Prx5 and requires a threonine and arginine residue to stabilize the transition state [3,32,33]. Residues Thr114 and Arg195 are conserved in *Pf*AOP [23], whereas a second arginine or a histidine residue, which were suggested to affect the oxidative half-reaction in Prx1-type [34] and Prx6-type [35,36]

Abbreviations: AOP, antioxidant protein; GR, glutathione reductase; Grx, glutaredoxin; GSH, reduced glutathione; *Pf*, *Plasmodium falciparum*; Prx, peroxiredoxin (s); tBOOH, *tert*-butyl hydroperoxide.

* Corresponding author. Fax: +49 6221 56 4643.
E-mail address: marcel.deponte@gmx.de (M. Deponte).

[1] These authors contributed equally to this work.

http://dx.doi.org/10.1016/j.freeradbiomed.2015.04.030

enzymes, respectively, are absent. In addition, *Pf*AOP has a second cysteine residue (Cys143) with unknown function [21]. This cysteine is found in a variety of Prx5-type homologues from bacteria, plants, and animals including human [21,37–39] (Fig. 1A). Since Cys143 is buried in the crystal structure of *Pf*AOP [23], we were surprised to detect its glutathionylation *in vitro* and in *Escherichia coli* [21]. SDS-PAGE redox mobility shift assays furthermore indicated a reversible as well as time- and concentration-dependent hydroperoxide- and GSH-dependent formation and reduction of an intramolecular disulfide bond between Cys117 and Cys143 *in vitro* [21]. Although Cys143 was shown to be nonessential for *Pf*AOP catalysis, its replacement with serine reduced the k_{cat}^{app} value and affected the enzyme kinetic patterns. This might be correlated with significant structural rearrangements that must be postulated to allow the formation of an intermolecular or intramolecular disulfide bond [21], as the sulfur atoms of Cys117 and Cys143 in the X-ray structure of *Pf*AOP are about 7.8 Å apart and are separated by the side chain of Leu109 at the bottom of the active site pocket [23] (Fig. 1B). Interestingly, the side chain of Leu109 adopts different conformations in subunits A and B of the crystallized homodimer (Figs. 1C,D). We therefore hypothesized that this residue might play a regulatory role as a gatekeeper that controls the accessibility of Cys143 [21]. Here we characterized the relevance of Leu109 and Cys143 for *Pf*AOP catalysis and suggest a novel mechanism for balancing the hydroperoxidase activity and inactivation susceptibility of Prx with implications for redox regulation.

Materials and methods

Site-directed mutagenesis, heterologous expression, and protein purification

Residue Leu109 of *Pf*AOP was replaced by site-directed mutagenesis according to a previously described protocol using the plasmids *PfAOP*/pQE30 and *PfAOP*^{C143S}/pQE30 as templates [21]. The mutagenesis primers are listed in Supplementary Table 1. Correct sequences of *PfAOP*^{L109A}, *PfAOP*$^{L109A/C143S}$, *PfAOP*^{L109V}, *PfAOP*$^{L109V/C143S}$, *PfAOP*^{L109M}, *PfAOP*$^{L109M/C143S}$, *PfAOP*^{L109Q}, and *PfAOP*$^{L109Q/C143S}$ were confirmed by sequencing both strands. Recombinant N-terminally MRGSH$_6$GS-tagged wild-type *Pf*AOP and single point mutants as well as the glutathione reductase *Pf*GR and the mutant glutaredoxin *Pf*Grx$^{C32S/C88S}$ were expressed in *Escherichia coli* strain XL1-Blue and purified by affinity chromatography as previously described [21,40]. Please note that the His-tag in *Pf*AOP is far away from the active site as well as the protein dimerization site [21] and therefore should not affect the enzymatic properties. Because the yields of the double mutants *Pf*AOP$^{L109A/C143S}$ and *Pf*AOP$^{L109Q/C143S}$ were rather low under standard expression conditions, all double mutants and the control *Pf*AOP^{C143S} were expressed overnight at 28 °C in the presence of 0.1 mM isopropyl-β-D-1-thiogalactopyranoside. Protein concentrations of the eluates were determined using the Bradford assay with bovine serum albumin as a standard [41]. Average yields for all *Pf*AOP mutants per liter of *E. coli* culture were between 0.6 μmol (13 mg) for *Pf*AOP^{L109Q} and 1.1 μmol (25 mg) for *Pf*AOP$^{L109V/C143S}$.

Steady-state kinetics

Standardized kinetic assays for the determination of the activities of *Pf*GR, *Pf*Grx$^{C32S/C88S}$, and *Pf*AOP were carried out at 25 °C using a thermostated Jasco V-650 UV-visual spectrophotometer as previously described [21,40,42]. Apparent k_{cat} and K_m values (k_{cat}^{app} and K_m^{app}) for *tert*-butyl hydroperoxide (tBOOH) were determined for wild-type and mutant *Pf*AOP in a coupled assay containing 150 μM NADPH, 1 mM GSH, 1 U/ml *Pf*GR, 5 μM *Pf*Grx$^{C32S/C88S}$, and 10 to 100 μM tBOOH. Activity measurements with 5 to 100 μM H_2O_2 were performed with 150 μM NADPH, 2 mM GSH, 1 U/ml *Pf*GR, and 2 μM *Pf*Grx$^{C32S/C88S}$, and the activity of a reference cuvette containing all assay components except for *Pf*AOP was subtracted. The assay concentration for wild-type and single mutant *Pf*AOP was 1.5 μM, except for *Pf*AOP^{L109M} (0.5 to 1 μM) and *Pf*AOP^{L109Q} (3 μM). Double mutants were assayed at an enzyme concentration of up to 10 μM for *Pf*AOP$^{L109Q/C143S}$. Kinetic data obtained from initial velocity measurements were analyzed as previously described [21].

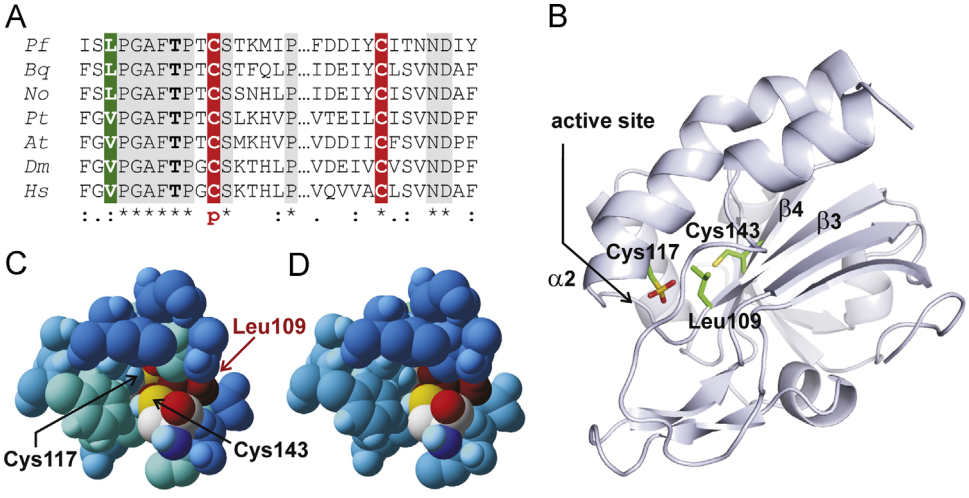

Fig. 1. The second cysteine residue and a potential gatekeeper of *Pf*AOP and Prx5 homologues. (A) Sequence alignment of Prx5 stretches comprising the peroxidatic cysteine residue, which is labeled with a "p," and the second cysteine residue, which is found in many bacterial and eukaryotic homologues. The potential gatekeeper residue is shaded in green. *Pf*, *P. falciparum*; *Bq*, *Bartonella quintana* (gi|49474601); *No*, *Nitrosococcus oceani* (gi|77164827); *Pt*, *Populus tremula* (PDB 1TP9); *At*, *Arabidopsis thaliana* (gi|21593881); *Dm*, *Drosophila melanogaster* (gi|78706776); *Hs*, *Homo sapiens* (PDB 2VL2). (B) Structure of *Pf*AOP chain A as ribbon diagram with the peroxidatic Cys117 at the beginning of helix α2, Leu109 at the end of β-strand 3, and Cys143 in β-strand 4 highlighted. (C) View along the two cysteine residues of *Pf*AOP toward the bottom of the active site pocket. Only selected residues (see Ref. [21]) of the crystal structure PDB entry 1XIY [23] are shown for clarity. The entry side for the hydroperoxide substrate is behind oxidized Cys117 and cannot be seen from the chosen perspective. Subunit A reveals a potential gate between both cysteines with the sulfur atom of Cys117 at the back pointing toward the sulfur atom of Cys143 at the front. The side chain of the potential gatekeeper Leu109 is depicted in dark red and adopts a partially "open" conformation. (D) Same view along the cysteine residues of subunit B with residue Leu109 adopting a rather "closed" conformation.

Protein crystallization and structure determination

Freshly purified *Pf*AOP^{L109M} was desalted on a PD-10 column with ice-cold buffer containing 30 mM Tris, 1 mM EDTA, HCl, pH 8.0, at 4 °C. The buffer was supplemented with 14.3 mM 2-mercaptoethanol before use. *Pf*AOP^{L109M} was crystallized by sitting drop vapor diffusion at 4 °C with a reservoir composition of 0.1 M sodium citrate, pH 5.6, 13% w/v PEG 4000, and 18% v/v 2-propanol. Crystallization drops contained 250 nl 15 mg/ml *Pf*AOP^{L109M} mixed with 500 nl reservoir solution. Data were collected at ESRF Grenoble beam line ID29 at 100 K, integrated using XDS [43], and scaled with AIMLESS [44,45]. Phases were obtained by molecular replacement using PHASER [46] with PDB entry 1XIY [23] as search model. Model building was done with COOT [47]. The structure was refined using PHENIX [48] without NCS restraints (Supplementary Table 2). Structure figures were created with PyMOL [49]. The atomic coordinates and structure factors have been deposited in the Research Collaboratory for Structural Bioinformatics Protein Data Bank under PDB code 4D73.

Results

Generation and purification of mutants

Before we replaced the potential gatekeeper Leu109 by site-directed mutagenesis, we performed an *in silico* analysis based on the published structure of *Pf*AOP in its sulfonic acid state [23]. Using the mutate tool of Swiss-Pdb viewer [50], we introduced either shorter or longer uncharged amino acids at position 109 in order to vary the diameter of the potential gate between Cys117 and Cys143. Please note that position 109 in the modeled structures allowed not only the accommodation of the shorter amino acid residues valine or alanine but also of the longer amino acid residues glutamine or methionine without steric hindrance. We therefore replaced Leu109 of recombinant *Pf*AOP and *Pf*AOP^{C143S} by site-directed mutagenesis and purified the wild-type and mutant enzymes *Pf*AOP^{L109A,V,M,Q} and *Pf*AOP$^{L109A,V,M,Q/C143S}$ (summarized as *Pf*AOP^{L109X}) by affinity chromatography. All proteins were stable and of high purity as revealed by SDS-PAGE (Supplementary Fig. 1). However, the hydroperoxidase activity decreased over time, resulting, for example, in a loss of approx. 50% activity of *Pf*AOP^{L109M} after 3 days of storage at 4 °C. All subsequent experiments were therefore performed with freshly purified enzyme.

Residue 109 and 143 both affect the hydroperoxidase kinetics

Wild-type enzyme and mutants of *Pf*AOP were analyzed in an established coupled enzymatic assay with tBOOH, GSH, and *Pf*Grx$^{C32S/C88S}$ as substrates (Fig. 2 and Supplementary Table 3). The mutant of *Pf*Grx was previously shown to be functional in the assay and was used in order to exclude Grx-dependent side reactions [21]. The activities of *Pf*AOP^{L109A} and *Pf*AOP^{L109V}, containing a shortened hydrophobic gatekeeper candidate, were significantly decreased, whereas the activity of *Pf*AOP^{L109M}, containing a longer hydrophobic gatekeeper candidate, was three times higher than the activity of the wild-type enzyme (Fig. 2A). The increased activity was not due to a direct oxidation of NADPH by *Pf*AOP^{L109M} as revealed by control experiments without *Pf*Grx$^{C32S/C88S}$ or *Pf*GR (data not shown) in accordance with previous results for the wild-type enzyme [21]. Hence, the hydroperoxidase activity of *Pf*AOP could be correlated with the length of residue 109 in descending order (Met > Leu > Val > Ala). Replacement of Leu109 by a long hydrophilic residue in *Pf*AOP^{L109Q} resulted in the lowest enzymatic activity (Fig. 2A), suggesting that not only the length but also the apolarity of the side chain is crucial.

In order to decipher a potential influence of Cys143 on the altered activities, we then analyzed the same mutations for *Pf*AOP^{C143S} (Fig. 2B). While the decreased activities for Ala109, Val109, and Gln109 in *Pf*AOP^{C143S} were comparable to the Cys143-containing mutants, the activating effect for Met109 was lost in *Pf*AOP$^{L109M/C143S}$. The data in Figs. 2A and B therefore indicate a Cys143-dependent and Cys143-independent influence of residue 109 on catalysis. This interpretation was supported by the kinetic patterns (Supplementary Fig. 2) and parameters (Fig. 2C and Supplementary Table 3): Linear regression analyses for *Pf*AOP^{L109M} and the wild-type enzyme yielded rather parallel lines in Lineweaver–Burk plots (Supplementary Fig. 2a), whereas all other mutants, including *Pf*AOP$^{L109M/C143S}$ and its control *Pf*AOP^{C143S}, appeared to have a common intersection point (Supplementary Figs. 2A,B). Thus, the mutation Met109 altered the correlation between the microscopic rate constants of the enzymatic reaction either in a comparable way to all the other gatekeeper mutants when Cys143 was absent (Supplementary Fig. 2B) or in an alternative way when Cys143 was present (Supplementary Fig. 2A). As indicated by the parallel lines in the Lineweaver–Burk plot, *Pf*AOP^{L109M} had a similar catalytic efficiency as the wild-type enzyme because of a threefold increased K_m^{app} *and* k_{cat}^{app} value. In contrast, an increase of the K_m^{app} value of all other mutants was coupled to a decrease of the k_{cat}^{app} value (Fig. 2C and Supplementary Table 3). In summary, the kinetic data reveal an important role of Leu109 for *Pf*AOP catalysis and support a functional coupling between the active site and Cys143 that is mediated with the help of the gatekeeper residue.

Residues 109 and 143 affect the susceptibility of the enzyme to inactivation

Prx from different species are well known for their inactivation during turnover [8,10,11,51]. When we monitored the initial hydroperoxidase activities of the *Pf*AOP^{L109X} mutants and the corresponding controls, we noted significant differences with regard to the time courses and inactivation kinetics (Fig. 3A). In order to analyze the inactivation, we normalized the time courses and compared the relative activities over the first 80 s during turnover. The activities of *Pf*AOP^{L109V} and wild-type *Pf*AOP decreased significantly faster during the assay than the activity of *Pf*AOP^{L109M} (Fig. 3B). Moreover, even though *Pf*AOP^{L109Q} had the lowest overall activity of the *Pf*AOP^{L109X} mutants (Fig. 2C), the replacement by glutamine resulted in the highest durability in the assay (Fig. 3B). A decreased inactivation was also observed for the long gatekeeper residues Met109 and Gln109 in the double mutants lacking Cys143. However, the effects were less pronounced because replacement of the second cysteine residue itself appeared to increase the enzyme durability during turnover (Fig. 3C). In summary, the presence of Cys143 could render *Pf*AOP more susceptible to tBOOH-dependent inactivation, and, regardless of the polarity and overall activity, long gatekeeper residues stabilize *Pf*AOP during catalysis.

Next, we tried to identify the inactivated enzyme species that accumulates in the tBOOH peroxidase assay. We previously detected the time- and concentration-dependent formation and reduction of disulfide-bridged species in the absence of either the oxidizing or the reducing substrate using redox mobility shift assays [21]. Attempts to monitor a potential accumulation of these oxidized *Pf*AOP species in the course of the enzymatic assay failed because the alkylation kinetics for unmodified cysteine residues were much too slow to become competitive in the presence of all substrates, which is a common methodological pitfall [6,52]. We therefore analyzed the reaction of *Pf*AOP with H_2O_2 as an

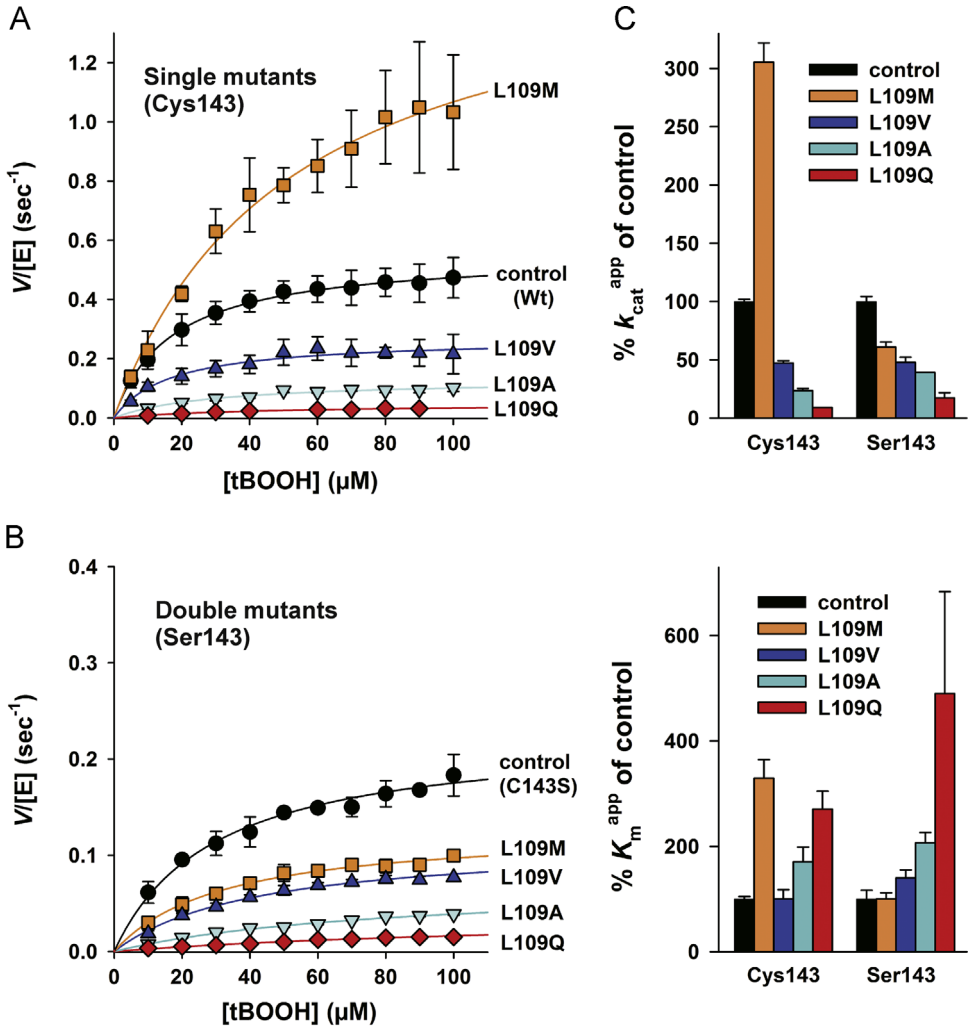

Fig. 2. Steady-state kinetics of *Pf*AOP^{L109X} mutants with tBOOH. (A) Michaelis–Menten plot of the hydroperoxidase activities of *Pf*AOP^{L109X} mutants in the presence of Cys143. The wild-type enzyme served as a control. (B) Michaelis–Menten plot of the hydroperoxidase activities of *Pf*AOP^{L109X} mutants lacking Cys143. *Pf*AOP^{C143S} served as a control. (C) Comparison of the kinetic parameters k_{cat}^{app} and K_m^{app} of *Pf*AOP^{L109X} mutants and controls from panels A and B. Absolute values are given in Supplementary Table 3. All values were determined with 1 mM GSH, 5 μM *Pf*Grx$^{C32S/C88S}$, and variable concentrations of tBOOH in the assay, and all data are the mean ± SD of three to five replicate measurements of at least two independent enzyme purifications.

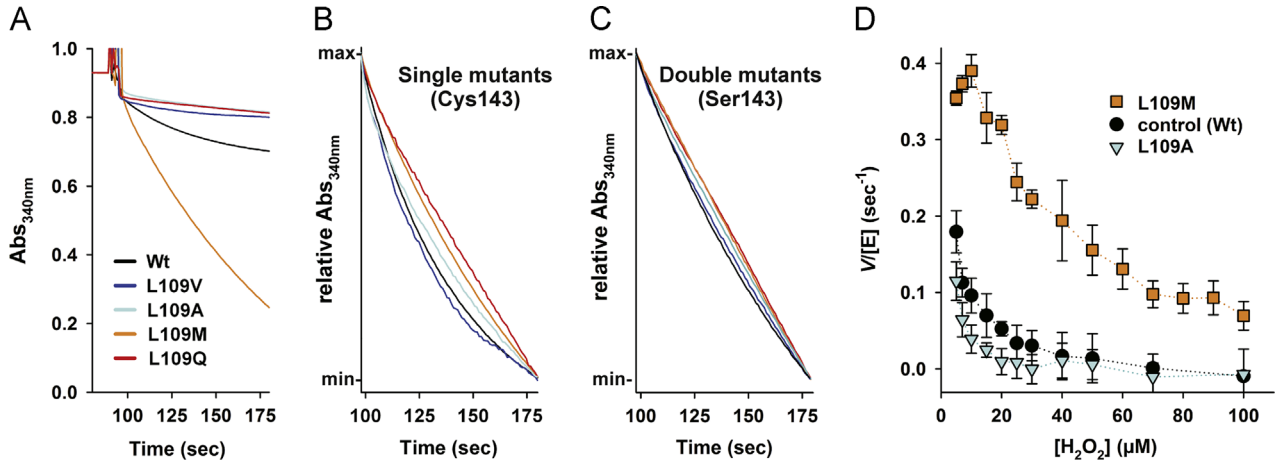

Fig. 3. Inactivation of *Pf*AOP^{L109X} mutants by tBOOH and H_2O_2. (A) Time course measurements with 100 μM tBOOH as hydroperoxide substrate. (B) Normalized activities of *Pf*AOP^{L109X} mutants with tBOOH in the presence of Cys143. The wild-type enzyme served as a control. For each time course measurement from panel (A), the absorbances at 100 and 180 s were set as the maximum (Abs_{max}) and minimum (Abs_{min}) absorbances, respectively. (C) Normalized activities of *Pf*AOP^{L109X} mutants lacking Cys143. *Pf*AOP^{C143S} served as a control. Relative absorbances were normalized as in panel B. (D) Michaelis–Menten plot of the hydroperoxidase activities of wild-type *Pf*AOP, *Pf*AOP^{L109A}, and *Pf*AOP^{L109M} with H_2O_2. Initial reaction velocities were determined within 5 s after the addition of enzyme, revealing a concentration-dependent inactivation of mutant and wild-type enzyme by H_2O_2. All data are the mean ± SD of at least four replicate measurements of two independent enzyme purifications.

alternative substrate. However, competitive quenching experiments with H_2O_2 and catalase [53] were also unsuccessful in monitoring the accumulation of oxidized *Pf*AOP because inactivation by H_2O_2 was even far more potent than inactivation by tBOOH as revealed by concentration–activity plots (Fig. 3D). It is interesting to note that neither wild-type nor mutant *Pf*AOP showed apparent Michaelis–Menten kinetics with H_2O_2 as a substrate. Instead, all enzymes were rapidly inactivated in a concentration-dependent manner (Fig. 3D). An initial increase of the peroxidase activity was only observed for *Pf*AOP^{L109M} at very low H_2O_2 concentrations, and *Pf*AOP^{L109M} was also the only enzyme with a decreased susceptibility to inactivation and a significant residual activity at 100 μM H_2O_2. In contrast, *Pf*AOP^{L109A} was even more efficiently inactivated than the wild-type enzyme. In summary, H_2O_2 is not only a substrate but also a potent inhibitor of *Pf*AOP that leads to enzyme inactivation. The susceptibility to inactivation depends on residue 109 and is partially compensated in *Pf*AOP^{L109M}.

Crystal structure of PfAOP^{L109M}

In order to gain a deeper understanding of the unexpected durability of *Pf*AOP^{L109M} and its increased k_{cat}^{app} value, we crystallized the mutant protein and solved its structure by molecular replacement at 1.8 Å resolution (Supplementary Table 2) (PDB entry 4D73). The overall structure was very similar to wild-type *Pf*AOP (PDB entry 1XIY [23]) with rmsd values of 0.26 and 0.22 Å for corresponding C_{alpha} atoms of chains A and B, respectively. As expected from modeling, in subunit A the active center is in a closed state and Met109 is located between Cys143 and "overoxidized" Cys117 (Fig. 4). Met109 adopts a frequently observed side chain conformation [54] and is in close contact with the side chain of Cys143, which was built with two alternative side chain conformations due to the observed, broadened electron density. Compared to the wild-type structure, the side chain of Cys143 is rotated away from Cys117 (Fig. 4, left panels). In contrast to subunit A, the peroxidatic Cys117 and the adjacent residues 115 to 119 of *Pf*AOP^{L109M} are disordered in subunit B, and the side chain of Met109 is not in contact with Cys143 (Fig. 4, right panels). The other residues in the vicinity of position 109 show very similar side chain conformations in both subunits of the wild-type and mutant structure (Supplementary Fig. 3). Please note that local unfolding of the active site is in general crucial for Prx catalysis because it allows the attack either of a resolving cysteine residue or of the reducing substrate, as previously demonstrated for a number of Prx isoforms [3,9,12–14,24,53,55–57]. Moreover, the different conformations of active sites A and B observed in *Pf*AOP^{L109M} are in accordance with the previously suggested negative subunit cooperativity for *Pf*AOP [21].

PfAOP^{L109M} has a very low K_m^{app} value for GSH

GSH is a true substrate of *Pf*AOP because Cys143 is nonessential for catalysis and *Pf*Grx$^{C32S/C88S}$ provides only one cysteine residue per catalytic cycle and therefore cannot regenerate a thiol from a sulfenic acid [21]. When we compared the activities of *Pf*AOP^{L109M}, *Pf*AOP^{L109A}, and wild-type enzyme at variable GSH concentrations, all proteins had biphasic kinetics as revealed by hyperbolic and linear regression analysis (Fig. 5A,B) in accordance with previous observations for *Pf*AOP and *Pf*AOP^{C143S} [21]. However, *Pf*AOP^{L109M} was saturated at much lower GSH concentrations with approx. 20- and 10-fold lower K_{m1}^{app} and K_{m2}^{app} values as compared with wild-type enzyme (Figs. 5B,C and Supplementary Table 4). Hence, the mutation Met109 drastically improved the apparent affinity of oxidized *Pf*AOP toward GSH, whereas the k_{cat1}^{app} and k_{cat2}^{app} values at variable GSH concentrations were only increased by approx. 40 and 20% under the chosen assay conditions. The effect of Met109 on the reductive half-reaction was specific for GSH, since *Pf*AOP^{L109M} and wild-type enzyme had similar K_m^{app} values for *Pf*Grx$^{C32S/C88S}$ (Fig. 6 and Supplementary Table 5), even though the k_{cat}^{app} value of *Pf*AOP^{L109M} at variable Grx concentrations was about 2.3 times higher as compared with wild-type enzyme. In summary, *Pf*AOP^{L109M} has a much higher apparent affinity for GSH but not for Grx as compared to wild-type enzyme.

Discussion

How do residue 109 and Cys143 alter *Pf*AOP catalysis, and how can we explain the significant gain of function for *Pf*AOP^{L109M}? During

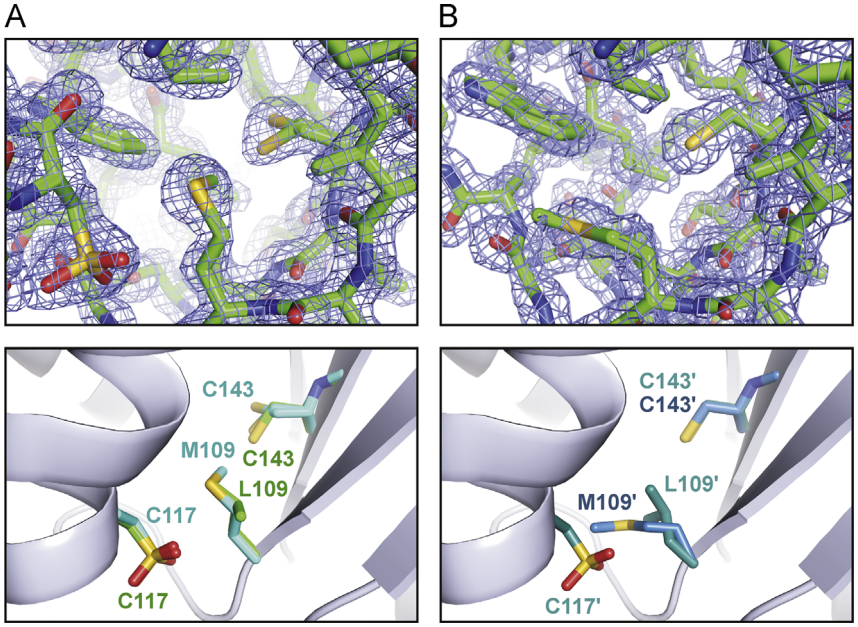

Fig. 4. Comparison of the X-ray structures of *Pf*AOP^{L109M} and wild-type *Pf*AOP. Chains A and B are shown on the left and right side, respectively. Residues 115–119 including Cys117 of *Pf*AOP^{L109M} are disordered in chain B and cannot be seen. Upper panels: electron density map at 1.5 σ contour level of *Pf*AOP^{L109M} with $2F_{obs}–F_{calc}$. Lower left panel: superposition of chain A of *Pf*AOP^{L109M} (light blue) and wild-type *Pf*AOP (green) with side chains shown for residues Leu/Met109, Cys117, and Cys143. Lower right panel: superposition of chain B of *Pf*AOP^{L109M} (blue) and wild-type *Pf*AOP (dark green).

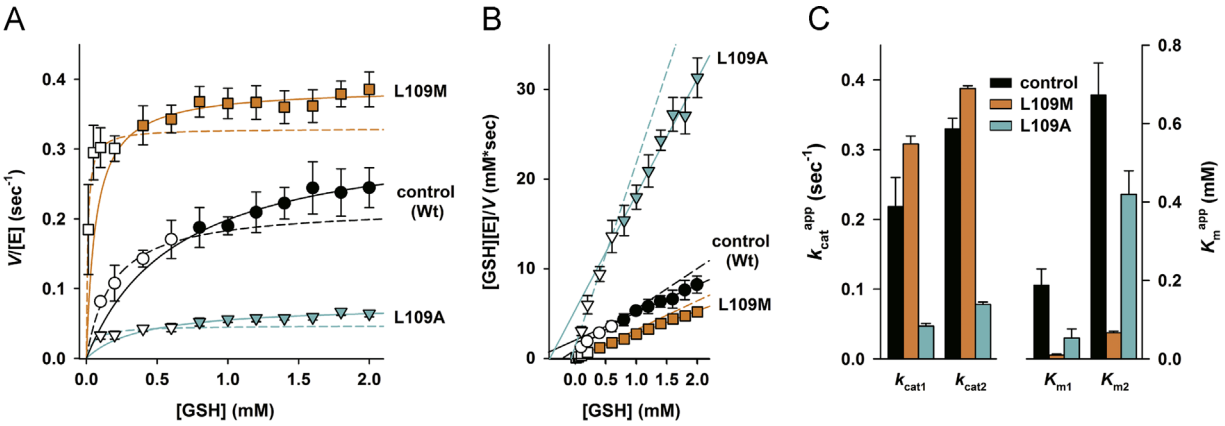

Fig. 5. Steady-state kinetics of *Pf*AOP^{L109X} mutants with GSH. (A) Michaelis–Menten plot showing the biphasic GSH-dependent hydroperoxidase activities of *Pf*AOP^{L109M}, *Pf*AOP^{L109A}, and wild-type *Pf*AOP with tBOOH. Closed and dashed lines indicate the hyperbolic fits for the values at high (closed symbols) and low (open symbols) GSH concentrations, respectively. (B) Hanes plot with -K_m^{app} values for GSH as *x*-intercepts. Closed and dashed lines indicate the linear fits for the data at high (closed symbols) and low (open symbols) GSH concentrations, respectively. (C) Comparison of the kinetic parameters k_{cat}^{app} and K_m^{app} (see also Supplementary Table 4). All values were determined with 75 μM tBOOH, 2 μM *Pf*Grx$^{C32S/C88S}$, and variable concentrations of GSH in the assay, and all data are the mean ± SD of three to six replicate measurements of at least three independent enzyme purifications.

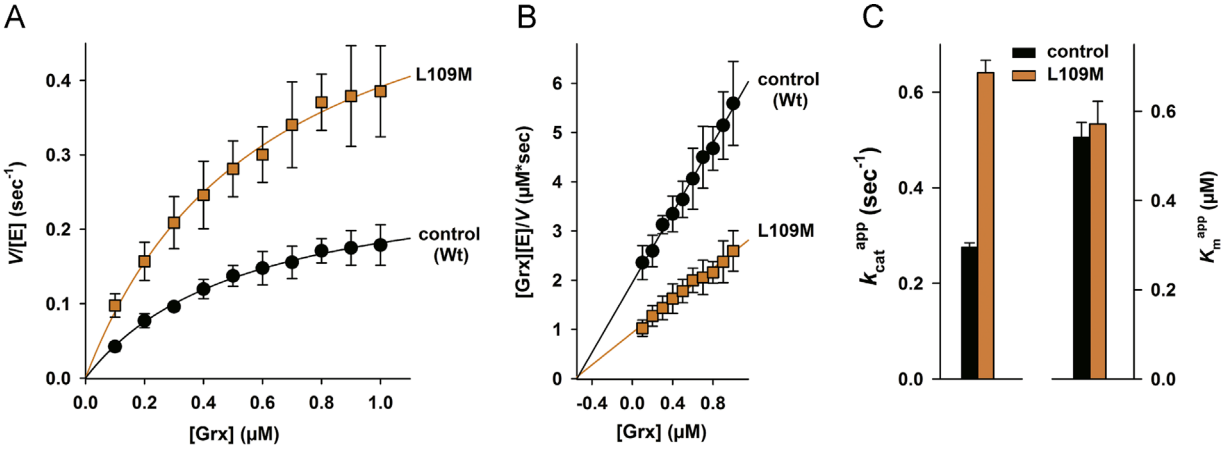

Fig. 6. Steady-state kinetics of *Pf*AOP^{L109M} and wild-type enzyme with *Pf*Grx$^{C32S/C88S}$. (A) Michaelis–Menten plot of the Grx-dependent hydroperoxidase activities with tBOOH. (B) Hanes plot with -K_m^{app} values for Grx as *x*-intercepts. (C) Comparison of the kinetic parameters k_{cat}^{app} and K_m^{app} (see also Supplementary Table 5). All values were determined with 75 μM tBOOH, 1 mM GSH, and variable concentrations of *Pf*Grx$^{C32S/C88S}$ in the assay, and all data are the mean ± SD of three to six replicate measurements of at least three independent enzyme purifications.

turnover Prx adopt a variety of redox states such as E-SH, E-SOH, and E-SSR (Fig. 7A). Moreover, E-SH and E-SOH exist in alternative conformations with a folded or locally unfolded helix α2 (E-SH$_{fo}$, E-SOH$_{fo}$, E-SOH$_{lu}$, and E-SH$_{lu}$) [3,10,13]. The peroxidatic cysteine residue is highly reactive and rapidly forms a sulfenic acid [15,33], presumably as soon as the hydroperoxide substrate adopts a correct orientation. Hence, the regeneration of the reduced enzyme, including conformational changes and the formation of E-SSR and E-SH$_{lu}$ (Fig. 7A), is probably rate limiting for many Prx [15,57,58]. Secondary plots from previous kinetic measurements with GSH revealed that the "true" k_{cat} of *Pf*AOP tends to be infinite [21]. Thus, it is probably impossible to saturate the enzyme–substrate complex between *Pf*AOP and GSH at high tBOOH and *Pf*Grx concentrations. In other words, binding and deprotonation of GSH and/or the adoption of a correct orientation between the oxidized enzyme and GSH might occur at a slower rate than disulfide bond formation and could be the rate-limiting step [57–59]. Our previous studies did not reveal whether GSH attacks E-SOH or a mixed disulfide between *Pf*AOP and *Pf*Grx [21]. Although we do not rule out the latter pathway, the data for *Pf*AOP^{L109M} rather support a model with GSH as the first reductant (Fig. 7B). A comparison of the crystal structures of wild-type *Pf*AOP and *Pf*AOP^{L109M} suggests that the replacement of Leu with Met at position 109 alters the balance between the fully folded and the locally unfolded conformation and has a destabilizing effect on the fully folded conformation, which results in a disordered active site in subunit B of *Pf*AOP^{L109M}. Hence, Met109 may alter the ratio of the microscopic rate constants k_3 and k_{-3} and accelerate local unfolding of helix α2. As a result, the steady-state concentration of E-SOH$_{lu}$ would increase (which could slow down the inactivation of *Pf*AOP as outlined below). In accordance with an increased E-SOH$_{lu}$ concentration, the drastically lowered K_m^{app} of *Pf*AOP^{L109M} for GSH might reflect more frequent successful encounters between the GSH and the enzyme. The unchanged K_m^{app} of *Pf*AOP^{L109M} for *Pf*Grx$^{C32S/C88S}$ also fits into this mechanistic model because E-SSG is trapped in the locally unfolded state and cannot isomerize to the folded state. Hence, binding of *Pf*Grx$^{C32S/C88S}$ on the protein surface does not depend on k_3/k_{-3} and the gatekeeper mutation. If the replacement of Leu^{109} with methionine also affects k_8/k_{-8}, the increased K_m^{app} of *Pf*AOP^{L109M} for tBOOH might analogously reflect a decreased steady-state concentration of E-SH$_{fo}$ that results in less frequent successful encounters between tBOOH and the enzyme. In addition, residue 109 at the bottom of the active site pocket should also affect the pK_a value and orientation of the peroxidatic cysteine in its folded conformation and therefore directly alter the reactivity with the peroxide substrate. A mechanistic coupling between the peroxidatic cysteine and Cys143 in accordance with our gatekeeper hypothesis is supported by two observations.

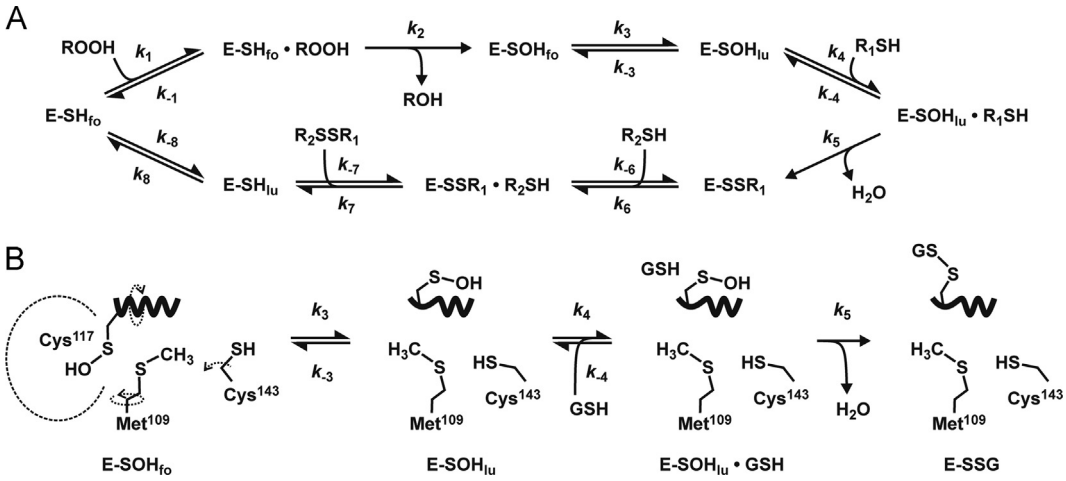

Fig. 7. Mechanistic model for *Pf*AOP catalysis. (A) General model for Prx catalysis. (B) Potential effects of residue 109 and the second cysteine residue on *Pf*AOP^{L109M} catalysis. The active site pocket where hydroperoxide reduction takes place is indicated by a dashed line. Crucial protonation and deprotonation steps are omitted for simplicity.

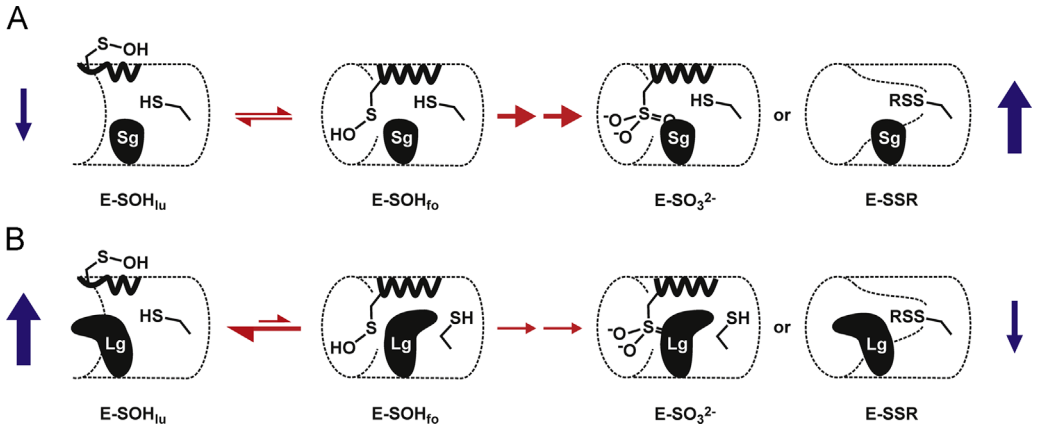

Fig. 8. Mechanistic model for *Pf*AOP inactivation with implications for potential redox sensing. Altered conformational dynamics (indicated by red arrows) and gatekeeper-dependent shielding of the second cysteine residue could affect the formation of the previously detected E-SSR species [21] or the formation of the sulfinic and sulfonic acid species as detected in the crystal structure (Fig. 4) [23] and by mass spectrometry [21]. (A) Short gatekeeper mutants (Sg) have a delayed unfolding of helix α2 and a less shielded second cysteine residue. As a result, turnover decreases, and the enzyme is more susceptible to inactivation. (B) Long gatekeeper constructs (Lg) have a promoted unfolding of helix α2 and a highly shielded second cysteine. As a result, turnover increases, and the enzyme has an increased durability. The altered ratio between active and inactive enzyme species in panels A and B is indicated by blue arrows.

First, the gain of function for Met109 requires the presence of Cys143 and, second, detrimental effects of the gatekeeper mutations are increased by the replacement of Cys143. One might speculate that the sulfur atom of Met109 results in an altered redox mechanism; however, the electron densities in the crystal structure and general chemical considerations rather speak against an involvement of a methionine sulfoxide, radical or homocysteine species. In summary, the combined influence of Cys143 and residue 109 on catalysis could be explained by a direct effect on the reactivity of the peroxidatic cysteine residue as well as indirect effects on the reaction with GSH because of altered conformational dynamics of helix α2.

If a single point mutation leads to a 20-fold decrease of the K_m^{app} value for the potentially rate-limiting substrate interaction and a threefold increase of the k_{cat}^{app} value, why is such a mutant not selected *in vivo* (i.e., in apicomplexan parasites or other organism with similar Prx5 homologues)? One of several plausible answers to this question could be that the optimization of the peroxidase function might result in the loss of another function. Prx isoforms have been suggested, and in several cases shown, to act not only as peroxidases but also as redox sensors [2,4–6,10,60,61]. The molecular basis of what makes Prx good redox sensors is not fully understood, and there are probably alternative mechanisms to balance alternative functions, depending on the Prx subfamily or individual enzyme. For several members of the Prx1-type subfamily the E-SOH$_{fo}$ species is stabilized by an YF motif close to the C-terminus. A delayed unfolding of helix α2 makes these enzymes more susceptible to the reaction with another peroxide substrate. The resulting overoxidized Prx is inactive and has altered protein-protein interactions [3,6,10,51,62]. Alternatively, the formation of particular E-SSR species was suggested as a common principle for redox sensing [4]. Examples for such species are the mixed disulfides between mammalian Prx1/2 and Ask1 [63], yeast Ahp1 and Cad1 [31], as well as yeast Prx1 and Trx3 [64]. Whether *Pf*AOP plays a role as a redox sensor is unknown; however, the efficient inactivation by H_2O_2 could point to this direction. As far as E-SSR formation is concerned, we previously detected a variety of *Pf*AOP species *in vitro* that might have suitable sensor properties [21]. The present study reveals that Cys143 and short gatekeeper residues make *Pf*AOP more susceptible to turnover-dependent inactivation, whereas long gatekeeper residues or the absence of Cys143 slow down inactivation. So far we could not specify the inactivated *Pf*AOP species that accumulates in the assay (despite a variety of experimental approaches). The two most likely and nonexclusive possibilities for inactivated *Pf*AOP are (i) E-SSR species and/or (ii) overoxidized species (Fig. 8). (i) As shown for *Pf*AOP^{L109M}, the shielding of the thiol group of Cys143 correlates with the length of the gatekeeper. A decreased shielding might facilitate the formation of the previously detected Cys143 disulfides [21] and could

therefore explain some of the altered inactivation properties. (ii) Since *Pf*AOP is structurally prone to overoxidation [23], different inactivation kinetics probably indicate an altered accumulation of the sulfinic or sulfonic acid states during turnover. As outlined above, the analyzed mutations presumably affect the unfolding dynamics of helix α2. Thus, the durability of the long gatekeeper mutants could be analogous to the durability of Prx1-type isoforms without the YF motif, and the susceptibility of the short gatekeeper mutants to inactivation could be caused by a delayed unfolding of helix α2 analogous to Prx1-type isoforms with a YF motif [3,10,51]. Regardless of the chemical nature of inactive *Pf*AOP, it remains to be shown whether the modulatory effects of Cys143 and the gatekeeper reflect a common balancing mechanism for catalysis and inactivation. Based on the decreased activity and slightly increased inactivation of the Val109 mutants, Prx5 homologues from plants, *Drosophila*, and human might be more susceptible to inactivation than bacterial Prx5 homologues, because the former enzymes have a valine instead of a leucine residue at the gatekeeper position (Fig. 1) [21]. If this is the case, the balancing mechanism would be the result of a convergent molecular evolution for Prx5-type and Prx1-type homologues. In summary, increased shielding of residue Cys143 by the gatekeeper and an accelerated unfolding of helix α2 are two nonexclusive models to explain the insensitivity of *Pf*AOP^{L109M} toward inactivation. A gain of function with regard to the hydroperoxidase activity and enzyme durability might be coupled to a loss of function for redox sensing *in vivo*.

In conclusion, our mutational analyses unraveled a modulatory effect of Cys143 and residue 109 on *Pf*AOP catalysis and inactivation. Both residues directly alter the reactivity of the peroxidatic cysteine toward the hydroperoxide substrate in the folded enzyme conformation. In addition, both residues appear to affect the local unfolding of helix α2 which inversely alters the susceptibility to enzyme inactivation and the reactivity toward GSH as the first reductant. The more robust and active enzyme *Pf*AOP^{L109M} might be interesting for the design of recombinant peroxidases. Furthermore, its gain of function *in vitro* might be detrimental *in vivo* because of a loss of function with regard to redox sensing. Future analysis will have to reveal whether the second cysteine residue and the Prx5-type subfamily of Prx are redox-regulated *in vivo*. The gatekeeper mutants described here might provide a useful tool for addressing this subject.

Author contributions

M.D. conceived the experiments. V.S., C.F.D., J.K., S.S., and M.B. performed the site-directed mutagenesis and enzymatic assays, M.D. purified the protein for protein crystallization trials, J.K. crystallized and solved the structure of *Pf*AOP^{L109M}, and all authors analyzed the data. M.D. wrote the manuscript and all authors checked and edited the manuscript.

Additional information

Accession codes: The atomic coordinates and structure factors for *Pf*AOP^{L109M} have been deposited under PDB code 4D73.

Acknowledgments

This work was supported by the Deutsche Forschungsgemeinschaft Grant DE 1431/8-1 (to M.D.). M.D. furthermore acknowledges the Deutsche Forschungsgemeinschaft for funding of his position in the frame of the Heisenberg program (Grant DE 1431/9-1). We thank Irmgard Sinning for stimulating discussions and Luise Krauth-Siegel for carefully reading the manuscript, and acknowledge Claudia Siegmann and Gabi Müller from the Cluster of Excellence:CellNetworks crystallization platform.

Appendix A. Supporting information

Supplementary data associated with this article can be found in the online version at http://dx.doi.org/10.1016/j.freeradbiomed.2015.04.030.

References

[1] Jang, H. H.; Lee, K. O.; Chi, Y. H.; Jung, B. G.; Park, S. K.; Park, J. H.; Lee, J. R.; Lee, S. S.; Moon, J. C.; Yun, J. W.; Choi, Y. O.; Kim, W. Y.; Kang, J. S.; Cheong, G. W.; Yun, D. J.; Rhee, S. G.; Cho, M. J.; Lee, S. Y. Two enzymes in one; two yeast peroxiredoxins display oxidative stress-dependent switching from a peroxidase to a molecular chaperone function. *Cell* **117:**625–635; 2004.

[2] Rhee, S. G.; Woo, H. A. Multiple functions of peroxiredoxins: peroxidases, sensors and regulators of the intracellular messenger H(2)O(2), and protein chaperones. *Antioxid. Redox Signal.* **15:**781–794; 2011.

[3] Hall, A.; Nelson, K.; Poole, L. B.; Karplus, P. A. Structure-based insights into the catalytic power and conformational dexterity of peroxiredoxins. *Antioxid. Redox Signal.* **15:**795–815; 2011.

[4] Brigelius-Flohe, R.; Flohe, L. Basic principles and emerging concepts in the redox control of transcription factors. *Antioxid. Redox Signal.* **15:**2335–2381; 2011.

[5] Edgar, R. S.; Green, E. W.; Zhao, Y.; van Ooijen, G.; Olmedo, M.; Qin, X.; Xu, Y.; Pan, M.; Valekunja, U. K.; Feeney, K. A.; Maywood, E. S.; Hastings, M. H.; Baliga, N. S.; Merrow, M.; Millar, A. J.; Johnson, C. H.; Kyriacou, C. P.; O'Neill, J. S.; Reddy, A. B. Peroxiredoxins are conserved markers of circadian rhythms. *Nature* **485:**459–464; 2012.

[6] Poynton, R. A.; Hampton, M. B. Peroxiredoxins as biomarkers of oxidative stress. *Biochim. Biophys. Acta* **1840:**906–912; 2014.

[7] Biteau, B.; Labarre, J.; Toledano, M. B. ATP-dependent reduction of cysteine-sulphinic acid by S. cerevisiae sulphiredoxin. *Nature* **425:**980–984; 2003.

[8] Koo, K. H.; Lee, S.; Jeong, S. Y.; Kim, E. T.; Kim, H. J.; Kim, K.; Song, K.; Chae, H. Z. Regulation of thioredoxin peroxidase activity by C-terminal truncation. *Arch. Biochem. Biophys.* **397:**312–318; 2002.

[9] Wood, Z. A.; Poole, L. B.; Hantgan, R. R.; Karplus, P. A. Dimers to doughnuts: redox-sensitive oligomerization of 2-cysteine peroxiredoxins. *Biochemistry* **41:**5493–5504; 2002.

[10] Wood, Z. A.; Poole, L. B.; Karplus, P. A. Peroxiredoxin evolution and the regulation of hydrogen peroxide signaling. *Science* **300:**650–653; 2003.

[11] Yang, K. S.; Kang, S. W.; Woo, H. A.; Hwang, S. C.; Chae, H. Z.; Kim, K.; Rhee, S. G. Inactivation of human peroxiredoxin I during catalysis as the result of the oxidation of the catalytic site cysteine to cysteine-sulfinic acid. *J. Biol. Chem.* **277:**38029–38036; 2002.

[12] Cao, Z.; Tavender, T. J.; Roszak, A. W.; Cogdell, R. J.; Bulleid, N. J. Crystal structure of reduced and of oxidized peroxiredoxin IV enzyme reveals a stable oxidized decamer and a non-disulfide-bonded intermediate in the catalytic cycle. *J. Biol. Chem.* **286:**42257–42266; 2011.

[13] Perkins, A.; Nelson, K. J.; Williams, J. R.; Parsonage, D.; Poole, L. B.; Karplus, P. A. The sensitive balance between the fully folded and locally unfolded conformations of a model peroxiredoxin. *Biochemistry* **52:**8708–8721; 2013.

[14] Haynes, A. C.; Qian, J.; Reisz, J. A.; Furdui, C. M.; Lowther, W. T. Molecular basis for the resistance of human mitochondrial 2-Cys peroxiredoxin 3 to hyperoxidation. *J. Biol. Chem.* **288:**29714–29723; 2013.

[15] Parsonage, D.; Nelson, K. J.; Ferrer-Sueta, G.; Alley, S.; Karplus, P. A.; Furdui, C. M.; Poole, L. B. Dissecting peroxiredoxin catalysis: separating binding, peroxidation, and resolution for a bacterial AhpC. *Biochemistry* **54:**1567–1575; 2015.

[16] Deponte, M.; Rahlfs, S.; Becker, K. Peroxiredoxin systems of protozoal parasites. *Subcell. Biochem* **44:**219–229; 2007.

[17] Kawazu, S.; Komaki-Yasuda, K.; Oku, H.; Kano, S. Peroxiredoxins in malaria parasites: parasitologic aspects. *Parasitol. Int.* **57:**1–7; 2008.

[18] Richard, D.; Bartfai, R.; Volz, J.; Ralph, S. A.; Muller, S.; Stunnenberg, H. G.; Cowman, A. F. A genome-wide chromatin-associated nuclear peroxiredoxin from the malaria parasite Plasmodium falciparum. *J. Biol. Chem.* **286:**11746–11755; 2011.

[19] Gretes, M. C.; Poole, L. B.; Karplus, P. A. Peroxiredoxins in parasites. *Antioxid. Redox Signal.* **17:**608–633; 2012.

[20] Koncarevic, S.; Rohrbach, P.; Deponte, M.; Krohne, G.; Prieto, J. H.; Yates 3rd J.; Rahlfs, S.; Becker, K. The malarial parasite *Plasmodium falciparum* imports the human protein peroxiredoxin 2 for peroxide detoxification. *Proc. Natl. Acad. Sci. USA* **106:**13323–13328; 2009.

[21] Djuika, C. F.; Fiedler, S.; Schnolzer, M.; Sanchez, C.; Lanzer, M.; Deponte, M. *Plasmodium falciparum* antioxidant protein as a model enzyme for a special class of glutaredoxin/glutathione-dependent peroxiredoxins. *Biochim. Biophys. Acta* **1830:**4073–4090; 2013.

[22] Djuika, C. F.; Huerta-Cepas, J.; Przyborski, J. M.; Deil, S.; Sanchez, C. P.; Doerks, T.; Bork, P.; Lanzer, M.; Deponte, M. Prokaryotic ancestry and gene fusion of a dual localized peroxiredoxin in malaria parasites. *Microbial Cell* **2:**5–13; 2015.

[23] Sarma, G. N.; Nickel, C.; Rahlfs, S.; Fischer, M.; Becker, K.; Karplus, P. A. Crystal structure of a novel *Plasmodium falciparum* 1-Cys peroxiredoxin. *J. Mol. Biol.* **346:**1021–1034; 2005.
[24] Karplus, P. A.; Hall, A. Structural survey of the peroxiredoxins. *Subcell. Biochem.* **44:**41–60; 2007.
[25] Knoops, B.; Goemaere, J.; Van der Eecken, V.; Declercq, J. P. Peroxiredoxin 5: structure, mechanism, and function of the mammalian atypical 2-Cys peroxiredoxin. *Antioxid. Redox Signal.* **15:**817–829; 2011.
[26] Zhou, Y.; Kok, K. H.; Chun, A. C.; Wong, C. M.; Wu, H. W.; Lin, M. C.; Fung, P. C.; Kung, H.; Jin, D. Y. Mouse peroxiredoxin V is a thioredoxin peroxidase that inhibits p53-induced apoptosis. *Biochem. Biophys. Res. Commun.* **268:**921–927; 2000.
[27] Banmeyer, I.; Marchand, C.; Clippe, A.; Knoops, B. Human mitochondrial peroxiredoxin 5 protects from mitochondrial DNA damages induced by hydrogen peroxide. *FEBS Lett.* **579:**2327–2333; 2005.
[28] Godoy, J. R.; Funke, M.; Ackermann, W.; Haunhorst, P.; Oesteritz, S.; Capani, F.; Elsasser, H. P.; Lillig, C. H. Redox atlas of the mouse. Immunohistochemical detection of glutaredoxin-, peroxiredoxin-, and thioredoxin-family proteins in various tissues of the laboratory mouse. *Biochim. Biophys. Acta* **1810:**2–92; 2011.
[29] De Simoni, S.; Linard, D.; Hermans, E.; Knoops, B.; Goemaere, J. Mitochondrial peroxiredoxin-5 as potential modulator of mitochondria-ER crosstalk in MPP+-induced cell death. *J. Neurochem.* **125:**473–485; 2013.
[30] Pauwels, F.; Vergauwen, B.; Van Beeumen, J. J. Physiological characterization of *Haemophilus influenzae* Rd deficient in its glutathione-dependent peroxidase PGdx. *J. Biol. Chem.* **279:**12163–12170; 2004.
[31] Iwai, K.; Naganuma, A.; Kuge, S. Peroxiredoxin Ahp1 acts as a receptor for alkylhydroperoxides to induce disulfide bond formation in the Cad1 transcription factor. *J. Biol. Chem.* **285:**10597–10604; 2010.
[32] Hall, A.; Parsonage, D.; Poole, L. B.; Karplus, P. A. Structural evidence that peroxiredoxin catalytic power is based on transition-state stabilization. *J. Mol. Biol.* **402:**194–209; 2010.
[33] Trujillo, M.; Clippe, A.; Manta, B.; Ferrer-Sueta, G.; Smeets, A.; Declercq, J. P.; Knoops, B.; Radi, R. Pre-steady state kinetic characterization of human peroxiredoxin 5: taking advantage of Trp84 fluorescence increase upon oxidation. *Arch. Biochem. Biophys.* **467:**95–106; 2007.
[34] Nagy, P.; Karton, A.; Betz, A.; Peskin, A. V.; Pace, P.; O'Reilly, R. J.; Hampton, M. B.; Radom, L.; Winterbourn, C. C. Model for the exceptional reactivity of peroxiredoxins 2 and 3 with hydrogen peroxide: a kinetic and computational study. *J. Biol. Chem.* **286:**18048–18055; 2011.
[35] Deponte, M.; Becker, K. Biochemical characterization of *Toxoplasma gondii* 1-Cys peroxiredoxin 2 with mechanistic similarities to typical 2-Cys Prx. *Mol. Biochem. Parasitol.* **140:**87–96; 2005.
[36] Nakamura, T.; Yamamoto, T.; Abe, M.; Matsumura, H.; Hagihara, Y.; Goto, T.; Yamaguchi, T.; Inoue, T. Oxidation of archaeal peroxiredoxin involves a hypervalent sulfur intermediate. *Proc. Natl. Acad. Sci. USA* **105:**6238–6242; 2008.
[37] Seo, M. S.; Kang, S. W.; Kim, K.; Baines, I. C.; Lee, T. H.; Rhee, S. G. Identification of a new type of mammalian peroxiredoxin that forms an intramolecular disulfide as a reaction intermediate. *J. Biol. Chem.* **275:**20346–20354; 2000.
[38] Declercq, J. P.; Evrard, C.; Clippe, A.; Stricht, D. V.; Bernard, A.; Knoops, B. Crystal structure of human peroxiredoxin 5, a novel type of mammalian peroxiredoxin at 1.5 A resolution. *J. Mol. Biol.* **311:**751–759; 2001.
[39] Rouhier, N.; Gelhaye, E.; Jacquot, J. P. Glutaredoxin-dependent peroxiredoxin from poplar: protein-protein interaction and catalytic mechanism. *J. Biol. Chem.* **277:**13609–13614; 2002.
[40] Urscher, M.; More, S. S.; Alisch, R.; Vince, R.; Deponte, M. Tight-binding inhibitors efficiently inactivate both reaction centers of monomeric *Plasmodium falciparum* glyoxalase 1. *FEBS J.* **279:**2568–2578; 2012.
[41] Bradford, M. M. A rapid and sensitive method for the quantitation of microgram quantities of protein utilizing the principle of protein-dye binding. *Anal. Biochem.* **72:**248–254; 1976.
[42] Mesecke, N.; Mittler, S.; Eckers, E.; Herrmann, J. M.; Deponte, M. Two novel monothiol glutaredoxins from *Saccharomyces cerevisiae* provide further insight into iron-sulfur cluster binding, oligomerization, and enzymatic activity of glutaredoxins. *Biochemistry* **47:**1452–1463; 2008.
[43] Kabsch, W. Xds. *Acta Crystallogr. D Biol. Crystallogr* **66:**125–132; 2010.
[44] Winn, M. D.; Ballard, C. C.; Cowtan, K. D.; Dodson, E. J.; Emsley, P.; Evans, P. R.; Keegan, R. M.; Krissinel, E. B.; Leslie, A. G.; McCoy, A.; McNicholas, S. J.; Murshudov, G. N.; Pannu, N. S.; Potterton, E. A.; Powell, H. R.; Read, R. J.; Vagin, A.; Wilson, K. S. Overview of the CCP4 suite and current developments. *Acta Crystallogr. D Biol. Crystallogr* **67:**235–242; 2011.
[45] Evans, P. R.; Murshudov, G. N. How good are my data and what is the resolution? *Acta Crystallogr. D Biol. Crystallogr* **69:**1204–1214; 2013.
[46] McCoy, A. J.; Grosse-Kunstleve, R. W.; Adams, P. D.; Winn, M. D.; Storoni, L. C.; Read, R. J. Phaser crystallographic software. *J. Appl. Crystallogr* **40:**658–674; 2007.
[47] Emsley, P.; Lohkamp, B.; Scott, W. G.; Cowtan, K. Features and development of Coot. *Acta Crystallogr. D Biol. Crystallogr* **66:**486–501; 2010.
[48] Adams, P. D.; Afonine, P. V.; Bunkoczi, G.; Chen, V. B.; Davis, I. W.; Echols, N.; Headd, J. J.; Hung, L. W.; Kapral, G. J.; Grosse-Kunstleve, R. W.; McCoy, A. J.; Moriarty, N. W.; Oeffner, R.; Read, R. J.; Richardson, D. C.; Richardson, J. S.; Terwilliger, T. C.; Zwart, P. H. PHENIX: a comprehensive Python-based system for macromolecular structure solution. *Acta Crystallogr. D Biol. Crystallogr* **66:**213–221; 2010.
[49] Schrodinger, LLC The PyMOL Molecular Graphics System, Version 1.3r1. 2010.
[50] Guex, N.; Peitsch, M. C. SWISS-MODEL and the Swiss-PdbViewer: an environment for comparative protein modeling. *Electrophoresis* **18:**2714–2723; 1997.
[51] Sayed, A. A.; Williams, D. L. Biochemical characterization of 2-Cys peroxiredoxins from *Schistosoma mansoni*. *J. Biol. Chem.* **279:**26159–26166; 2004.
[52] Winther, J. R.; Thorpe, C. Quantification of thiols and disulfides. *Biochim. Biophys. Acta* **1840:**838–846; 2014.
[53] Evrard, C.; Capron, A.; Marchand, C.; Clippe, A.; Wattiez, R.; Soumillion, P.; Knoops, B.; Declercq, J. P. Crystal structure of a dimeric oxidized form of human peroxiredoxin 5. *J. Mol. Biol.* **337:**1079–1090; 2004.
[54] Lovell, S. C.; Word, J. M.; Richardson, J. S.; Richardson, D. C. The penultimate rotamer library. *Proteins* **40:**389–408; 2000.
[55] Hirotsu, S.; Abe, Y.; Okada, K.; Nagahara, N.; Hori, H.; Nishino, T.; Hakoshima, T. Crystal structure of a multifunctional 2-Cys peroxiredoxin heme-binding protein 23 kDa/proliferation-associated gene product. *Proc. Natl. Acad. Sci. USA* **96:**12333–12338; 1999.
[56] Kim, S. J.; Woo, J. R.; Hwang, Y. S.; Jeong, D. G.; Shin, D. H.; Kim, K.; Ryu, S. E. The tetrameric structure of *Haemophilus influenza* hybrid Prx5 reveals interactions between electron donor and acceptor proteins. *J. Biol. Chem.* **278:**10790–10798; 2003.
[57] Deponte, M. Glutathione catalysis and the reaction mechanisms of glutathione-dependent enzymes. *Biochim. Biophys. Acta* **1830:**3217–3266; 2013.
[58] Flohe, L.; Toppo, S.; Cozza, G.; Ursini, F. A comparison of thiol peroxidase mechanisms. *Antioxid. Redox Signal.* **15:**763–780; 2011.
[59] Toppo, S.; Flohe, L.; Ursini, F.; Vanin, S.; Maiorino, M. Catalytic mechanisms and specificities of glutathione peroxidases: variations of a basic scheme. *Biochim. Biophys. Acta* **1790:**1486–1500; 2009.
[60] Cho, C. S.; Yoon, H. J.; Kim, J. Y.; Woo, H. A.; Rhee, S. G. Circadian rhythm of hyperoxidized peroxiredoxin II is determined by hemoglobin autoxidation and the 20S proteasome in red blood cells. *Proc. Natl. Acad. Sci. USA* ; 2014.
[61] O'Neill, J. S.; Reddy, A. B. Circadian clocks in human red blood cells. *Nature* **469:**498–503; 2011.
[62] Peskin, A. V.; Dickerhof, N.; Poynton, R. A.; Paton, L. N.; Pace, P. E.; Hampton, M. B.; Winterbourn, C. C. Hyperoxidation of peroxiredoxins 2 and 3: rate constants for the reactions of the sulfenic acid of the peroxidatic cysteine. *J. Biol. Chem.* **288:**14170–14177; 2013.
[63] Jarvis, R. M.; Hughes, S. M.; Ledgerwood, E. C. Peroxiredoxin 1 functions as a signal peroxidase to receive, transduce, and transmit peroxide signals in mammalian cells. *Free Radic. Biol. Med.* **53:**1522–1530; 2012.
[64] Greetham, D.; Kritsiligkou, P.; Watkins, R. H.; Carter, Z.; Parkin, J.; Grant, C. M. Oxidation of the yeast mitochondrial thioredoxin promotes cell death. *Antioxid. Redox Signal.* **18:**376–385; 2013.